Vitamin E succinate mediated apoptosis by juxtaposing endoplasmic reticulum and mitochondria

Manobendro Nath Ray[a], Michiko Kiyofuji[b], Mizune Ozono[b] and Kentaro Kogure[b]*

[a]Department of Pharmaceutical Health Chemistry, Graduate School of Pharmaceutical Sciences, Tokushima University, 1–78–1 Shomachi, Tokushima 770-8505, Japan

[b]Graduate School of Biomedical Sciences, Tokushima University, 1–78–1 Shomachi, Tokushima 770-8505, Japan

*Corresponding author: Kentaro Kogure

Department of Pharmaceutical Health Chemistry, Graduate School of Biomedical Sciences, Tokushima University, Shomachi 1, Tokushima 770-8505, Japan
TEL: +81-88-633-7248 FAX: +81-88-633-9572
Email: kogure@tokushima-u.ac.jp

Abstract

Vitamin E succinate (VES) is an esterified form of natural α-tocopherol, has turned out to be novel anticancer agent. However, its anticancer mechanisms have not been illustrated. Previously, we reported VES mediated Ca^{2+} release from the endoplasmic reticulum (ER) causes mitochondrial Ca^{2+} overload, leading to mitochondrial depolarization and apoptosis. Here, we elucidated the mechanism of VES-induced Ca^{2+} transfer from ER to mitochondria by investigating the role of VES in ER-mitochondria contact formation. Transmission electron microscopic observation confirms VES mediated ER-mitochondria contact while fluorescence microscopic analysis revealed that VES increased mitochondria-associated ER membrane (MAM) formation. Pre-treatment with the inositol 1,4,5-triphosphate receptor (IP_3R) antagonist 2-aminoethyl diphenylborinate (2-APB) decreased VES-induced MAM formation, suggesting the involvement of VES-induced Ca^{2+} efflux from ER in MAM formation. The ER IP_3R receptor is known to interact with voltage-dependent anion channels (VDAC) via the chaperone glucose-regulated protein 75 kDa (GRP75) to bring ER and mitochondria nearby. Although we revealed that VES treatment does not affect GRP75 protein level, it increases GRP75 localization in the MAM. In addition, the inhibition of Ca^{2+} release from ER by 2-APB decreases GRP75 localization in the MAM, suggesting the possibility of Ca^{2+}-induced conformational change of GRP75 that promotes formation of the IP_3R-GRP75-VDAC complex and thereby encourages MAM formation. This study identifies the mechanism of VES-induced enhanced Ca^{2+} transfer from ER to mitochondria, which causes mitochondrial Ca^{2+} overload leading to apoptosis.

Keywords: Vitamin E succinate; GRP75; ER-mitochondria contact; Ca^{2+} transfer; Apoptosis

1. Introduction

The apoptosis pathway has been acknowledged as a promising target for the prevention of cancer recurrence and metastasis for over three decades [1,2]. Inter-organelle communication, and particularly structural and functional interactions between the endoplasmic reticulum (ER) and mitochondria, is an emerging aspect of cellular processes and signaling pathways that influence cellular apoptosis [3]. The membranes of ER and mitochondria can interact with each other and form an interface of approximately 10 nm, which is known as the mitochondria-associated ER membrane (MAM). MAM serves as a complex hub that influences various essential cellular pathways such as lipid synthesis, Ca^{2+} exchange, mitochondrial DNA replication, apoptosis, and autophagy [4–7].

Factors leading to the formation of MAM are under investigation. The inositol 1,4,5-trisphosphate receptor (IP_3R), the main Ca^{2+}-releasing channel on the ER membrane, is known to form a complex with voltage-dependent anion channels (VDAC) in the outer mitochondrial membrane. Formation of this complex in the MAM also involves the chaperone glucose-regulated protein 75 kDa (GRP75), which has emerged as an important contributor to mitochondrial homeostasis [8]. GRP75 is primarily located in the mitochondrial matrix, but a low level of GRP75 is found in the cytoplasm and nucleus [9]. GRP75 thus can act as a link between IP_3R and VDAC and enable the juxtaposition of ER and mitochondria to regulate Ca^{2+} transfer between these organelles. The mediation of the coupling between ER and mitochondria by GRP75 has been shown to cause Ca^{2+}-dependent apoptosis in cancer and diabetic retinopathy [10,11].

Proper assembly of these proteins in the MAM enhances the contact between ER and mitochondria and creates a microdomain of high Ca^{2+} concentration, which is necessary

to allow uptake by the low-affinity mitochondrial Ca^{2+} uniporter. Ca^{2+} transfer from ER to mitochondria is crucial for mitochondrial ATP production, division and metabolism as well as pathophysiological processes including apoptosis, carcinogenesis, and metastasis [12,13]. Accordingly, reduced MAM formation and the resulting decrease of ER-mitochondrial Ca^{2+} transfer has been shown to contribute to carcinogenesis and to resistance to chemotherapy, radiotherapy and molecularly targeted drugs [14,15]. Consequently, the ER-mitochondria interplay related to Ca^{2+} transfer has recently emerged as an area of intense cancer research, especially with regard to the induction of apoptosis [16].

The number of anticancer agents approved by the US Food and Drug Administration (FDA) that target apoptotic pathways is limited [2]. Therefore, novel apoptosis-inducing agents are needed to support the development of anticancer therapies. Recently, vitamin E succinate (VES), a fat-soluble succinyl ester of natural α-tocopherol (Fig. 1A). VES is not an antioxidant like vitamin E. The phenolic hydroxyl group of vitamin E is an active site of antioxidation. The replacement of the hydroxyl group by the ester group causes loss of its antioxidant activity. Recently, it was identified as a promising anticancer agent that interacts with apoptotic machinery [17]. However, the apoptotic mechanisms of VES are complex and have not yet been completely elucidated.

The primary function of ER is to fold the misfolded proteins into their functional conformation. However, oncogene activation, loss of tumour suppressors, hypoxia, nutrient deprivation, and acidosis cause the generation of misfolded proteins in cancer cells [18]. The chaperone system and protein degradation system make the in-house protein quality control (PQC) system of the cell that controls the number of misfolded

proteins within the cells. Gene mutation, hostile microenvironment, inflammation, and rapid reactive oxygen species (ROS) production in cancer cells make PQC defective. The lack of clearance of misfolded proteins due to the dysfunctional PQC of the cancer cells, misfolded proteins accumulate within the cells. These defective proteins impose huge workload on ER leading to ER stress.

VES has been proposed to cause apoptosis by inducing oxidative stress and ER stress [19–25]. Previously, we demonstrated that VES-induced apoptosis in cancer cells is caused, at least in part, by the induction of mitochondrial Ca^{2+} overload through the enhancing of Ca^{2+} transfer from ER to mitochondria [26]. Because Ca^{2+} transfer from ER to mitochondria critically depends on the distance between these two organelles [27], and due to its hydrophobic nature [28] it may easily reach out to different organelles like ER and mitochondria, we propose that VES may improve the inter-organelle contact between ER and mitochondria and that this effect may contribute to apoptosis in cancer cells. However, direct evidence of presence of VES in ER is unavailable. Apart from its anticancer activity, it has some other promising biological activities like the inhibition of cholinesterase activity, inhibition of nuclear factor kappa-B activation, enhancement of liposaccharide induced nitric oxide production [29].

Because of the significance of GRP75 to ER-mitochondrial dynamics and to Ca^{2+}-induced apoptosis, we hypothesized that VES might enhance ER-mitochondria contact by regulating the expression of GRP75 or its localization to MAM. To investigate this hypothesis, we examined the effect of VES on ER-mitochondria contact and GRP75 expression and localization in a cancer cell line. We were able to gain insight into the mechanism of VES-induced enhanced Ca^{2+} transfer from ER to mitochondria, which causes apoptosis in cancer cells.

2. Materials and methods

2.1. Chemicals

VES and egg phosphatidylcholine were purchased from Sigma-Aldrich (St. Louis, MO, USA). D-α-Tocopherol was purchased from Tokyo Chemical Industry (Tokyo, Japan). Other reagents were of the highest grade commercially available.

2.2. Liposome preparation

A chloroform solution (0.1 mL) containing 0.1 M VES was mixed with 0.64 mL of a chloroform solution containing egg phosphatidylcholine (0.1 g/mL) in a glass tube. The mixture was evaporated to dryness under a nitrogen stream to form a lipid film. The lipid film was hydrated with 192 μL PBS and 8 μL 1 N NaOH. The hydrated lipid film was incubated at 55 °C for 10 min in a water bath. After the incubation, the tube was sonicated in an ultrasonic bath for 10 to 15 min to form liposomes. The size and surface charge of the liposomes were measured with a Zetasizer Nano (Malvern Panalytical Ltd., UK).

2.3. Cell culture

Mouse melanoma B16F1 cells were purchased from American Type Culture Collection and were cultured in Dulbecco's modified Eagle medium (DMEM) containing 10% fetal bovine serum (FBS) and 1% penicillin-streptomycin at 37 °C in a 5% CO_2 humidified environment. When the cells reached 80% confluency, they were treated with VES for 6 h. For 2-APB-treated cells, 50 μM 2-APB was added 30 minutes prior to VES treatment.

2.4. Measurement of mitochondrial Ca^{2+}

After treatment with VES-containing liposomes and 2-APB, cells were washed twice with 0.5 mL PBS and then incubated with 2 mL culture medium containing 500 nM MitoTracker (#8778, Cell Signaling Technology, Danvers, MA, USA) for 30 min at 37 °C. After 30 min, 1 mL of medium was removed, and each dish was loaded with 1 mL Fluo-4 AM reagent containing 0.04% Pluronic F-127 and 1.25 mmol/L probenecid and incubated for 1 h at 37 °C. After incubation, cells were observed with an LSM700 confocal laser scanning microscope (Carl Zeiss, Oberkochen, Germany). At least 30 images were analyzed during each observation. Quantitative analysis was performed by drawing region of interest (ROI) boundaries around 15 to 22 cells per image and measuring the intensity of the yellow signal in the area with the "color threshold" function of ImageJ.

For the Rhodamine 2-AM assay, after treatment with VES-containing liposomes and 2-APB, cells were washed twice with 0.5 mL PBS and loaded with 1 mL Rhod 2-AM (#R002, DOJINDO LABORATORIES, Kumamoto, Japan) reagent containing 10 μM Rhod 2-AM, 0.05% Pluronic F-127 and 4 mmol/L probenecid and incubated for 1 h at 37 °C. After incubation, cells were observed with an LSM700 confocal laser scanning microscope. At least 30 images were analyzed during each observation. Quantitative analysis was performed by drawing region of interest (ROI) boundaries around 15 to 22 cells per image and measuring the green fluorescence intensity using ImageJ.

2.5. Analysis of ER-mitochondria contact

After treatment with VES-containing liposomes and 2-APB, cells were washed twice with 0.5 mL PBS. The cells were then incubated with 500 nM MitoTracker for 30 min at 37 °C and then fixed with 4% paraformaldehyde in PBS for 15 min at 37 °C. Following three washes with PBS containing 1% bovine serum albumin (BSA), cells

were permeabilized for 15 min at 37 °C with a PBS solution containing 1% BSA and 0.1% Triton X-100. The cells were washed and incubated with 1 mL culture medium containing 1 µL Cytopainter detection reagent (ab139482, Abcam) for 30 min at 37 °C. Following several washes with assay buffer from the Cytopainter kit, nuclei were counterstained for 15 min with DAPI solution (1 µg/mL). The cells were washed with PBS and observed with an LSM700 confocal laser scanning microscope. Quantitative analyses were performed by drawing ROI boundaries around 4 or 5 cells per image and measuring the intensity of the yellow signal in the area with the "color threshold" function of ImageJ. At least 30 images were analyzed during each observation.

2.6. Transmission electron microscopy (TEM)

Electron microscopic observation was performed by Tokai Electron Microscope Inc (Nagoya, Japan). Cells were seeded in a 35 mm dish, and after 24 h, VES was added and incubated for 6 h. Then, the medium was removed, and cells were pre-fixed with 2% paraformaldehyde (PFA) and 2% glutaraldehyde (GA) in 0.1M phosphate buffer (PB), pH7.4. After cooling at 4 °C, pre-fixation solution was replaced with 2% GA in 0.1M PB and incubated overnight at 4 °C. Post-fixation was done with 2% osmium tetroxide (OsO_4) in 0.1 M PB at 4 °C for 1 h. After dehydrating cells with ethanol, resin embedding was done using a 5:5 mixture of ethanol and resin (Quetol-812; Nisshin EM Co., Tokyo, Japan) at 60 °C for 48 h. 70-nm ultrathin sections were prepared from the embedded blocks using a diamond knife on an ultramicrotome (Ultracut UCT; Leica, Vienna, Austria). After incubation with 2% Uranyl acetate for 15 min at room temperature, the sections were treated with lead stain solution (Sigma-Aldrich Co.,) for 3 min at room temperature for electron staining. Stained sections were observed, and images were acquired with a CCD camera (EM-14830RUBY2; JEOL Ltd., Tokyo,

Japan) equipped transmission electron microscope (JEM-1400Plus; JEOL Ltd., Tokyo, Japan) at a pressurized voltage of 100 kV.

2.7. Real-time PCR

Total RNA was extracted and purified from cells with NucleoSpin RNA isolation and purification kit (Takara Bio, Otsu, Japan) according to the manufacturer's instructions. The total RNA concentration was determined with a Nanodrop 8000 spectrometer (Thermo Fisher Scientific, Waltham, MA, USA). Then, cDNA was synthesized from 200 ng of total RNA with PrimeScript RT Master Mix (Perfect Real Time; Takara Bio) using an MJ Mini Personal Thermal Cycler (Bio-Rad, Hercules, CA, USA). The reverse transcription reaction was performed at 37 °C for 15 min and 85 °C for 5 s. Real-time PCR analysis was performed using TB Green™ Premix Ex Taq™ II (Tli RNaseH Plus; Takara Bio) and a Thermal Cycler Dice Real-Time System III (Takara Bio). To analyze the mRNA levels of the genes encoding GRP75 and GAPDH, the cDNA was denatured at 95 °C for 30 s, followed by 40 cycles of 95 °C for 5 s and 60 °C for 30 s for amplification. The sequences of the primers used for the real-time PCR for mouse *HSP9A* gene (forward, 5′-GCGTCTTATTGGACGACGAT-3′; reverse, 5′-TGGCCCGTAATTTTCTGC-3′) and mouse *GAPDH* gene (forward, 5′-GAGGACCAGGTTGTCTCCTG-3′; reverse, 5′-ATGTAGGCCATGAGGTCCAC-3′). The level of mRNA corresponding to GRP75 was calculated using the $2^{-\Delta\Delta Ct}$ method by normalization relative to *GAPDH*.

2.8. Western blotting

The following antibodies were used: anti-GRP75 rabbit monoclonal antibody (3593S, Cell Signaling Technology), anti-β actin rabbit polyclonal (ab8227, Abcam), and anti-

horseradish peroxidase (HRP)-conjugated goat anti-rabbit IgG polyclonal antibody (A24531; Thermo Fisher Scientific). To observe the expression of GRP75 in VES and 2-APB treated cells, total protein (10 μg) was separated with 10% SDS-PAGE, and the proteins were electrophoretically transferred to a polyvinylidene difluoride membrane (Bio-Rad). The membrane was incubated with 5% skim milk dissolved in Tris-buffered saline (pH 7.4) containing 0.1% Tween-20 for 1 h at 37 °C, then with an anti-GRP75 antibody (1:3000) for 24 h at 4 °C. The membrane was washed and incubated with the HRP-conjugated secondary antibody at a dilution of 1:4000 for 1 h at 37 °C. After incubation of the membrane with a chemiluminescent substrate reagent (ECL Prime; GE Healthcare, Little Chalfont, UK), bands were detected with an LAS-4000 mini system (Fuji Film, Tokyo, Japan). The membrane was then washed three times for 45 minutes with Tris-buffered saline (pH 7.4) containing 0.1% Tween 20, incubated with an anti-β actin antibody (1:3000) for 24 h at 4 °C, and developed as above. Band intensities were quantified using ImageJ.

2.9. Immunostaining for GRP75 localization

After treatment with VES-containing liposomes and 2-APB, cells were washed twice with 0.5 mL PBS and then fixed with 4% paraformaldehyde in PBS for 15 min at 37 °C. Following three washes with PBS containing 1% BSA, cells were permeabilized for 15 min at 37 °C with a PBS solution containing 1% BSA and 0.1% Triton X-100. The cells were washed and incubated with primary antibody (anti-GRP75, diluted 1:200 in 1% BSA/PBS) for 1 h at 37 °C. Following several washes, goat anti-rabbit IgG labeled with Alexa Fluor 488 (ab150077, Abcam; diluted 1:200 in 1% BSA/PBS) was added, and the cells were incubated for 1 h at 37 °C. After incubation, the cells were washed three times with 1% BSA/PBS and incubated with 1 mL culture medium containing 1 μL

Cytopainter detection reagent for 30 min at 37 °C, and the cells were observed with an LSM700 confocal laser scanning microscope. Images obtained from the green and red channels were separately processed for background subtraction with a rolling ball radius of 50 pixels. The resulting images were converted to 16-bit images, and ROI boundaries were drawn around 7 to 10 cells per image. The ratios of colocalization of the Cytopainter and GRP75 signals were obtained as Pearson's correlation coefficients using the "colocalization finder" function of ImageJ. At least 30 images were analyzed during each observation.

2.10. Statistical analysis

Statistical significance was determined using one-way ANOVA and the Kruskal-Wallis test to compare multiple groups, followed by Tukey's honestly significant difference test and the Dunn test using JASP software. *P* values less than 0.05 were considered to indicate statistical significance.

3. Results

3.1. Effect of VES on mitochondrial Ca^{2+}

Previously, we proposed that mitochondrial Ca^{2+} overload is responsible for the induction of apoptosis in cancer cells by VES [26]. In the present study, to confirm the effect of VES on mitochondrial Ca^{2+} levels, we used a dual staining technique, in which we stained the mitochondria of mouse melanoma B16F1 cells with a mitochondria-specific dye, MitoTracker (red), and intracellular Ca^{2+} was detected using the Ca^{2+}-activated cell-permeable dye Fluo-4 (green). The yellow fluorescence in the merged images represents the mitochondrial Ca^{2+} level (Fig. 1B). Upon quantification of the yellow fluorescence by the color threshold method of image analysis, we found that VES-treated cells exhibited an increased yellow fluorescence intensity of 157 ± 9% relative to control (Fig. 1C). However, the yellow fluorescence intensity was decreased to 128 ± 3% of control in cells treated with both VES and the IP_3R antagonist 2-APB. In addition, we evaluated mitochondrial Ca^{2+} using mitochondria specific Ca^{2+} indicator Rhodamine 2-AM. We found that VES treated cells exhibited higher fluorescence representing mitochondrial Ca^{2+} while compared with control and 2-APB treated cells (Fig. 2A). On the contrary, pre-treatment of 2-APB restored VES induced increase of fluorescence intensity to the control level. Upon quantification, we found VES-treated cells exhibited an increased fluorescence intensity of 137 ± 10% relative to control (Fig. 2B). However, the fluorescence intensity was decreased to 107 ± 8% of control in cells treated with both VES and 2-APB.

3.2. Effect of VES on formation of contact sites between ER and mitochondria

The influence of the IP_3R receptor inhibitor 2-APB on VES induced mitochondrial Ca^{2+} overload suggested an involvement of the ER in the mitochondrial Ca^{2+} level. Therefore,

to investigate the effect of VES on formation of sites of contact between the ER and mitochondria, we treated B16F1 cells with VES with or without co-treatment with 2-APB. After 6 h of treatment, we stained mitochondria with MitoTracker (red) and ER with Cytopainter (green). The yellow fluorescence in the merged images represents the co-localization of mitochondria- and ER-specific fluorescence signals and is considered to indicate regions of ER-mitochondria contact. We observed that B16F1 cells treated with only VES showed higher yellow fluorescence compared to control cells. In contrast, the level of yellow fluorescence was similar in control cells and in cells treated with 2-APB alone (Fig. 3A). However, 2-APB treatment reduced the level of yellow fluorescence in VES-treated cells.

Upon quantification of the yellow fluorescence with the color threshold method, we found that the yellow fluorescence of VES-treated cells was approximately 167% that of control cells (Fig. 3B), while treatment with 2-APB alone did not cause a change in the intensity of yellow fluorescence compared to control. In contrast, the yellow fluorescence intensity was approximately 102% of control in cells treated with both 2-APB and VES. In addition, TEM analysis of VES treated B16F1 cells allowed us to observe the VES induced ER-mitochondria contact formation (Fig. 4A). Upon quantification of the extent of ER-mitochondria contact in VES treated group relative to control using image analysis, we found VES caused a significant reduction in distance between ER and Mitochondria compared to control (Fig. 4B).

3.3. Effect of VES on GRP75 expression

The formation of the IP_3R–GRP75–VDAC complex is known to enhance the ER–mitochondria interaction; changes to the expression of GRP75 thus represent one mechanism by which ER-mitochondria interactions may be altered. Therefore, we

performed real-time PCR to examine the influences of treatments involving VES and 2-APB on the expression of GRP75 in B16F1 cells. The level of mRNA expressed from the gene coding for GRP75, *HSP9A*, was normalized to that of the housekeeping gene *GAPDH* so as to control for cytotoxic effects. We found that the normalized level of *HSP9A* mRNA was higher in VES-treated B16F1 cells as compared to control (Fig. 5A). Conversely, the level of *HSP9A* mRNA was lower in 2-APB-treated cells relative to both control and VES-treated cells. The normalized level of *HSP9A* mRNA in VES-treated B16F1 cells was approximately 122% of that in control cells. In contrast, *HSP9A* mRNA was approximately 71% of control in cells treated with 2-APB alone. In addition, pre-treatment of VES-treated cells with 2-APB reduced the level of *HSP9A* mRNA level to approximately 96% that of control. We also assessed expression of GRP75 protein by western blotting. GRP75 protein showed an increased tendency in both VES- and 2-APB treated cells (Fig. 5B and Fig. 5C).

3.4. Effect of VES on GRP75 localization

Generally, GRP75 is most abundant in the mitochondrial matrix, but a low level of GRP75 is also found in the cytoplasm and nucleus [15]. To investigate the changes in GRP75 localization in the MAM upon treatment with VES and 2-APB, we performed a dual-staining technique, where GRP75 protein was detected with an anti-GRP75 antibody (green), and ER was detected with the ER-specific dye Cytopainter (red) in B16F1 cells after 3 h of treatment with the agents (Fig. 6A). We observed the tubular network of the ER and colocalization of GRP75 protein with ER (Fig. 6A, magnified). Here, the yellow signal in merged images represents the co-localization of GRP75 with ER; the co-localization of mitochondria-resident GRP75 with ER indicates the presence of GRP75 in the MAM. We observed that VES-treated B16F1 cells showed higher

yellow fluorescence compared to the control, while 2-APB treatment reduced the VES-induced increment of yellow fluorescence.

The amount of co-localization was quantified by determining the Pearson's correlation coefficients of the cells. In VES-treated cells, the median value of the Pearson's correlation coefficient was 0.86 (IQR 0.84-0.88), while in control cells, the median value of the Pearson's correlation coefficient was 0.75 (IQR 0.73-0.76) (Fig. 6B). However, when the cells were treated with both 2-APB and VES, the median value of the Pearson's correlation coefficient was 0.76 (IQR 0.75-0.77).

3.5. Effect of VES on apoptosis induction

Previously we confirmed VES induced apoptosis by evaluating loss of mitochondrial membrane potential by VES while pretreatment of 2-APB prevents VES induced mitochondrial membrane potential loss [26]. To further confirm VES induced apoptosis in our experimental model we observed morphological changes of the DAPI stained nucleus. We found morphological changes in nucleus of the VES treated cells compared to control (Fig. 7A). In addition, pre-treatment of 2APB prevented VES induced morphological changes of the nucleus. We calculated the percentage of apoptotic nucleus in different treatment groups, and we found around 35% apoptotic nucleus in VES treated B16F1 cells relative to control while pretreatment of 2-APB significantly reduced the percentage of VES induced apoptotic nucleus to control level (Fig. 7B). Nevertheless, TEM analysis of VES treated cells revealed cell shrinkage, chromatin condensation of the nucleus and cytoplasmic vacuoles (Fig. 7C).

4. Discussion

Vitamin E (VE) is well-known potent fat-soluble natural antioxidant. For decades, it was known that VE only works as a scavenger of lipid peroxyl radicals, specifically, oxidized low-density lipoprotein (oxLDL). Thus, it serves as a chief antioxidant for the prevention of atherosclerosis [30]. Recently, researchers found that VE is not only possess antioxidant activity, but also has pro-oxidant, cell signaling and gene regulatory functions. In addition, VE is effectively used for the prevention and treatment of heart disease, Alzheimer's disease, and chronic kidney disease [31,32]. While VE has no anticancer activity, its succinic acid ester derivative VES possess excellent anticancer potential.

We proposed VES induced elevation of intracellular calcium is one of the events in VES induced apoptosis [26]. In addition, we previously found some portion (5%) of VES was hydrolyzed in our experimental condition [26]. Hence, there is possibility of presence of VE in VES treated cells. Therefore, to confirm whether VE contributes to the elevation of intracellular calcium, we additionally performed experiment to evaluate effect of VE on intracellular calcium level. We found that treatment with 50 μM and 75 μM α-tocopherol did not show any change in Ca^{2+} specific fluorescence compared to control (Supplementary Fig. 1). Although VES induced intracellular Ca^{2+} was reported in our previous study [26]. These results suggest that VE does not induce ER stress like VES. Hence, there is no possibility of occurring the same phenomenon as VES in VE treated cancer cells.

Recently, we reported an intriguing relationship between the ER and mitochondria in the induction of apoptosis by VES [26], in that VES induces apoptosis in cancer cells by altering the flux of Ca^{2+} from ER to mitochondria. However, the mechanism mediating this Ca^{2+} flux was unknown. Notably, interactions between ER and

mitochondria increase following ER stress [33], and VES is known to induce ER stress. Therefore, we hypothesized that the influence of VES on ER-to-mitochondria Ca^{2+} flux may occur via increasing contact between these organelles or by inducing the formation MAM.

To test our hypothesis, we first examined the effect of VES on mitochondrial Ca^{2+} levels to confirm the induction of Ca^{2+} overload. We found increased fluorescence intensity representing mitochondrial Ca^{2+} in VES-treated cells compared to the control (Fig. 1B-C and Fig. 2), confirming that VES induced Ca^{2+} overload in mitochondria. TEM analysis of VES treated cells revealed cell shrinkage, chromatin condensation of the nucleus and cytoplasmic vacuoles confirming apoptosis (Fig. 7C). Again, pre-treatment of IP3R antagonist 2-APB prevents VES induced mitochondrial Ca^{2+} overload and apoptosis (Figs. 1, 2 and 7A-B) indicating involvement of VES induced Ca^{2+} overload in apoptosis induction.

While this overload has been demonstrated previously, the effect of VES on the MAM, the major region for Ca^{2+} exchange between the ER and mitochondria, had not been investigated. To test our hypothesis, we investigated the effect of VES on the MAM, the major region for Ca^{2+} exchange between the ER and mitochondria to determine how VES regulates Ca^{2+} transfer from ER to mitochondria to activate apoptosis. We found that VES treatment increases ER-mitochondria contact, which is indicative of the MAM formation, in B16F1 cells (Fig. 3A). In addition, we observed shorter distance between ER and mitochondria in VES treated cells compared to control in TEM analysis (Fig. 4) that provides further evidence of VES induced ER-mitochondria contact formation. However, pre-treatment with 2-APB, which is an IP3R antagonist that inhibits Ca^{2+} efflux from the ER, also diminished the VES-induced increase in MAM formation (Fig. 3B). These findings suggest that Ca^{2+} efflux from ER is essential for MAM formation.

GRP75 is a heat shock protein 70 (HSP70)-family chaperone that aids MAM formation by binding to both IP_3R and VDAC channels. Thus, we sought to determine whether VES manipulates the protein level of GRP75 and thus enhancing ER-mitochondria contact formation by treatment with VES. We found that mRNA encoding GRP75 increased upon VES treatment, while 2-APB treatment decrease mRNA levels to the control level in VES treated cells (Fig. 5). However, as determined by western blotting, we found no significant difference of GRP75 protein level among different groups. These results suggest that VES does not affect GRP75 protein level. In addition, Ca^{2+} efflux from ER does not influence GRP75 protein levels, and VES-induced upregulation of GRP75 protein thus is not likely to be responsible for VES-induced MAM formation. However, VES induced GRP75 translocation to the MAM region could be the possible reason of VES induced enhanced MAM formation. The primary cellular localization of GRP75 is mitochondria [34]. In addition, it is well established that GRP75 forms physical link between ER and mitochondria and aids MAM formation. We also confirmed VES induced decrease in ER-mitochondria proximity. Hence, there is possibility of finding more mitochondria resident GRP75 protein near to ER when mitochondria and ER comes closer upon VES treatment.

We did find a strong colocalization of GRP75 with ER in VES-treated cells (Pearson's correlation coefficient value = 0.86; Fig. 6B). We also found a positive correlation coefficient value (R^2 = 0.9863) which indicates a strong positive correlation between GRP75 fluorescence intensity and its western blot band intensity (Supplementary Fig. 2). Taken together, colocalization suggests that VES may act by altering the localization of GRP75 around ER, rather than influencing its expression. However, this result does not provide conclusive evidence of VES induced enhanced localization of GRP75 in the MAM region.

Ca^{2+} plays a crucial role in signal transduction by binding and changing the conformation of proteins [35]. In addition, Ca^{2+} is found to involved in folding and stabilization of some toxin proteins [36,37]. It has been reported that human HSP70 chaperone family proteins bind to two Ca^{2+} ions within the N-terminal ATPase domain [38]. Taken together, these findings suggest the possibility that Ca^{2+} released from ER may bind with GRP75 protein and change its conformation, thus aiding IP_3R–GRP75–VDAC complex formation. This hypothesis is supported by the decreases in ER-mitochondria contact and in GRP75 co-localization with ER seen when VES-treated cells are pre-treated with 2-APB (Fig. 3 and Fig. 6). However, further investigations are required to determine whether GRP75 is a Ca^{2+}-binding protein and to fully characterize the mechanism underlying VES-induced MAM formation.

Ryanodine receptors (RyR) are also located in the ER membrane. However, the responsiveness of RyR in MAM is less discussed by the researchers. This could be because the RyR creates Ca^{2+} microdomains with a short lifetime that limits the Ca^{2+} uptake through the low affinity mitochondrial uniporter (MCU) [39]. On the contrary, IP3R is physically connected to voltage-dependent anion channels (VDAC) via GRP75. It creates Ca^{2+} microdomain that maintains a Ca^{2+} concentration higher than cytosol. Thus IP3R-GRP75-VDAC microdomain overcomes low-affinity Ca^{2+} uptake properties of the mitochondrial Ca^{2+} uniporter complex [40]. It is difficult to say the exact fraction of Ca^{2+} released by IP3R channel that directly cleared by mitochondria. However, it can be said that IP3R contributes to the major fraction of Ca^{2+} taken up by mitochondria.

In summary, this is the first study to demonstrate that VES induces contact between ER and mitochondria possibly by enhancing the formation of IP_3R–GRP75–VDAC complexes via stimulation of Ca^{2+} efflux from ER. The increased contact between these

organelles facilitates the flow of Ca^{2+} from ER to mitochondria causing mitochondrial Ca^{2+} overload and leading to apoptosis. Accordingly, the IP_3R–GRP75–VDAC complex may be a promising target for cancer treatment.

Acknowledgements

This work was supported by a Research Programme for the Development of an Intelligent Tokushima Artificial Exosome (iTEX) from Tokushima University.

References

[1] B. Lim, Y. Greer, S. Lipkowitz, N. Takebe, Novel apoptosis-inducing agents for the treatment of cancer, a new arsenal in the toolbox, Cancers (Basel). 11 (2019) 1–39. https://doi.org/10.3390/cancers11081087.

[2] B.A. Carneiro, W.S. El-Deiry, Targeting apoptosis in cancer therapy, Nat. Rev. Clin. Oncol. 17 (2020) 395–417. https://doi.org/10.1038/s41571-020-0341-y.

[3] J. Rieusset, The role of endoplasmic reticulum-mitochondria contact sites in the control of glucose homeostasis: An update, Cell Death Dis. 9 (2018) 1–12. https://doi.org/10.1038/s41419-018-0416-1.

[4] M. Hamasaki, N. Furuta, A. Matsuda, A. Nezu, A. Yamamoto, N. Fujita, H. Oomori, T. Noda, T. Haraguchi, Y. Hiraoka, A. Amano, T. Yoshimori, Autophagosomes form at ER-mitochondria contact sites, Nature. 495 (2013) 389–393. https://doi.org/10.1038/nature11910.

[5] S. Marchi, S. Patergnani, P. Pinton, The endoplasmic reticulum–mitochondria connection: One touch, multiple functions, Biochim. Biophys. Acta - Bioenerg. 1837 (2014) 461–469. https://doi.org/10.1016/J.BBABIO.2013.10.015.

[6] D. Martinvalet, The role of the mitochondria and the endoplasmic reticulum contact sites in the development of the immune responses, Cell Death Dis. 9 (2018). https://doi.org/10.1038/s41419-017-0237-7.

[7] F. Giamogante, E. Poggio, L. Barazzuol, A. Covallero, T. Calì, Apoptotic signals at the endoplasmic reticulum-mitochondria interface, Adv. Protein Chem. Struct. Biol. 126 (2021) 307–343.https://doi.org/10.1016/BS.APCSB.2021.02.007.

[8] G. Szabadkai, K. Bianchi, P. Várnai, D. De Stefani, M.R. Wieckowski, D. Cavagna, A.I. Nagy, T. Balla, R. Rizzuto, Chaperone-mediated coupling of endoplasmic reticulum and mitochondrial Ca2+ channels, J. Cell Biol. 175

(2006) 901–911. https://doi.org/10.1083/jcb.200608073.

[9] Q. Ran, R. Wadhwa, R. Kawai, S.C. Kaul, R.N. Sifers, R.J. Bick, J.R. Smith, O.M. Pereira-Smith, Extramitochondrial Localization of Mortalin/mthsp70/PBP74/GRP75, Biochem. Biophys. Res. Commun. 275 (2000) 174–179. https://doi.org/10.1006/BBRC.2000.3237.

[10] S. Tiwary, A. Nandwani, R. Khan, M. Datta, GRP75 mediates endoplasmic reticulum–mitochondria coupling during palmitate-induced pancreatic β-cell apoptosis, J. Biol. Chem. 297 (2021) 101368. https://doi.org/10.1016/J.JBC.2021.101368.

[11] J. Li, F. Qi, H. Su, C. Zhang, Q. Zhang, Y. Chen, P. Chen, L. Su, Y. Chen, Y. Yang, Z. Chen, S. Zhang, GRP75-faciliated Mitochondria-associated ER Membrane (MAM) Integrity controls Cisplatin-resistance in Ovarian Cancer Patients, Int. J. Biol. Sci. 18 (2022) 2914–2931. https://doi.org/10.7150/ijbs.71571.

[12] L. Modesti, A. Danese, V. Angela, M. Vitto, D. Ramaccini, G. Aguiari, R. Gaf, G. Lanza, C. Giorgi, P. Pinton, Mitochondrial Ca 2 + Signaling in Health , Disease and Therapy, (2021) 1–30.

[13] Y. Zhang, Y. Wu, M. Zhang, Z. Li, B. Liu, H. Liu, J. Hao, X. Li, Synergistic mechanism between the endoplasmic reticulum and mitochondria and their crosstalk with other organelles, Cell Death Discov. 9 (2023) 1–10. https://doi.org/10.1038/s41420-023-01353-w.

[14] M.P.K. and S.H. Eric C. Meyers, Bleyda R. Solorzano, Justin James, Patrick D. Ganzer, Elaine S., Robert L. Rennaker, Balancing ER-mitochondrial Ca2+ fluxes in health and disease, Physiol. Behav. 176 (2018) 100–106. https://doi.org/10.1016/j.tcb.2021.02.003.Balancing.

[15] J. Çoku, D.M. Booth, J. Skoda, M.C. Pedrotty, J. Vogel, K. Liu, A. Vu, E.L.

Carpenter, J.C. Ye, M.A. Chen, P. Dunbar, E. Scadden, T.D. Yun, E. Nakamaru-Ogiso, E. Area-Gomez, Y. Li, K.C. Goldsmith, C.P. Reynolds, G. Hajnoczky, M.D. Hogarty, Reduced ER–mitochondria connectivity promotes neuroblastoma multidrug resistance, EMBO J. 41 (2022) 1–20. https://doi.org/10.15252/embj.2021108272.

[16] M. Kerkhofs, M. Bittremieux, G. Morciano, C. Giorgi, P. Pinton, J.B. Parys, G. Bultynck, Emerging molecular mechanisms in chemotherapy: Ca2+ signaling at the mitochondria-associated endoplasmic reticulum membranes, Cell Death Dis. 9 (2018). https://doi.org/10.1038/s41419-017-0179-0.

[17] L. Liang, L. Qiu, Vitamin E succinate with multiple functions: A versatile agent in nanomedicine-based cancer therapy and its delivery strategies, Int. J. Pharm. 600 (2021) 120457. https://doi.org/10.1016/J.IJPHARM.2021.120457.

[18] F. Tameire, I.I. Verginadis, C. Koumenis, Cell intrinsic and extrinsic activators of the unfolded protein response in cancer: Mechanisms and targets for therapy, Semin. Cancer Biol. 33 (2015) 3–15. https://doi.org/10.1016/j.semcancer.2015.04.002.

[19] K. Kogure, M. Morita, S. Nakashima, S. Hama, A. Tokumura, K. Fukuzawa, Superoxide is responsible for apoptosis in rat vascular smooth muscle cells induced by α-tocopheryl hemisuccinate, Biochim. Biophys. Acta - Gen. Subj. 1528 (2001) 25–30. https://doi.org/10.1016/S0304-4165(01)00168-4.

[20] L.F. Dong, P. Low, J.C. Dyason, X.F. Wang, L. Prochazka, P.K. Witting, R. Freeman, E. Swettenham, K. Valis, J. Liu, R. Zobalova, J. Turanek, D.R. Spitz, F.E. Domann, I.E. Scheffler, S.J. Ralph, J. Neuzil, α-Tocopheryl succinate induces apoptosis by targeting ubiquinone-binding sites in mitochondrial respiratory complex II, Oncogene. 27 (2008) 4324–4335.

https://doi.org/10.1038/onc.2008.69.

[21] G.A.S. Dos Santos, R.S. Abreu E Lima, C.R. Pestana, A.S.G. Lima, P.S. Scheucher, C.H. Thomé, H.L. Gimenes-Teixeira, B.A.A. Santana-Lemos, A.R. Lucena-Araujo, F.P. Rodrigues, R. Nasr, S.A. Uyemura, R.P. Falcão, H. De Thé, P.P. Pandolfi, C. Curti, E.M. Rego, (+)α-Tocopheryl succinate inhibits the mitochondrial respiratory chain complex I and is as effective as arsenic trioxide or ATRA against acute promyelocytic leukemia in vivo, Leukemia. 26 (2012) 451–460. https://doi.org/10.1038/leu.2011.216.

[22] K. Kluckova, A. Bezawork-Geleta, J. Rohlena, L. Dong, J. Neuzil, Mitochondrial complex II, a novel target for anti-cancer agents, Biochim. Biophys. Acta - Bioenerg. 1827 (2013) 552–564. https://doi.org/10.1016/j.bbabio.2012.10.015.

[23] B. Yan, M. Stantic, R. Zobalova, A. Bezawork-Geleta, M. Stapelberg, J. Stursa, K. Prokopova, L. Dong, J. Neuzil, Mitochondrially targeted vitamin E succinate efficiently kills breast tumour-initiating cells in a complex II-dependent manner, BMC Cancer. 15 (2015) 1–12. https://doi.org/10.1186/s12885-015-1394-7.

[24] X. Huang, Z. Zhang, L. Jia, Y. Zhao, X. Zhang, K. Wu, Endoplasmic reticulum stress contributes to vitamin E succinate-induced apoptosis in human gastric cancer SGC-7901 cells, Cancer Lett. 296 (2010) 123–131. https://doi.org/10.1016/j.canlet.2010.04.002.

[25] X. Huang, L. Li, L. Zhang, Z. Zhang, X. Wang, X. Zhang, L. Hou, K. Wu, Crosstalk between endoplasmic reticulum stress and oxidative stress in apoptosis induced by α-tocopheryl succinate in human gastric carcinoma cells, Br. J. Nutr. 109 (2013) 727–735. https://doi.org/10.1017/S0007114512001882.

[26] M.N. Ray, M. Ozono, M. Nakao, S. Sano, K. Kogure, Only one carbon difference determines the pro-apoptotic activity of α -tocopheryl esters, FEBS J. 290 (2022) 1027–1048. https://doi.org/10.1111/febs.16623.

[27] G. Csordás, P. Várnai, T. Golenár, S. Roy, G. Purkins, T.G. Schneider, T. Balla, G. Hajnóczky, Imaging Interorganelle Contacts and Local Calcium Dynamics at the ER-Mitochondrial Interface, Mol. Cell. 39 (2010) 121–132. https://doi.org/10.1016/j.molcel.2010.06.029.

[28] F. Bonina, M. Lanza, L. Montenegro, L. Salerno, P. Smeriglio, D. Trombetta, A. Saija, Transport of alpha-tocopherol and its derivatives through erythrocyte membranes., Pharm. Res. 13 (1996) 1343–1347. https://doi.org/10.1023/a:1016017832146.

[29] K. Kogure, D. Majima, R. Mitsuhashi, T. Fukuta, T. Tanaka, Biological functions of α-tocopheryl succinate, J. Nutr. Sci. Vitaminol. (Tokyo). 65 (2019) S104–S108. https://doi.org/10.3177/jnsv.65.S104.

[30] J.M. Tucker, D.M. Townsend, Alpha-tocopherol: roles in prevention and therapy of human disease., Biomed. Pharmacother. 59 (2005) 380–387. https://doi.org/10.1016/j.biopha.2005.06.005.

[31] F. Galli, M. Bonomini, D. Bartolini, L. Zatini, G. Reboldi, G. Marcantonini, G. Gentile, V. Sirolli, N. Di Pietro, Vitamin E (Alpha-Tocopherol) Metabolism and Nutrition in Chronic Kidney Disease, Antioxidants. 11 (2022) 1–19. https://doi.org/10.3390/antiox11050989.

[32] R. Brigelius-Flohé, Bioactivity of vitamin E, Nutr. Res. Rev. 19 (2006) 174–186. https://doi.org/10.1017/S0954422407202938.

[33] R. Bravo, J.M. Vicencio, V. Parra, R. Troncoso, J.P. Munoz, M. Bui, C. Quiroga, A.E. Rodriguez, H.E. Verdejo, J. Ferreira, M. Iglewski, M. Chiong, T.

Simmen, A. Zorzano, J.A. Hill, B.A. Rothermel, G. Szabadkai, S. Lavandero, Increased ER-mitochondrial coupling promotes mitochondrial respiration and bioenergetics during early phases of ER stress, J. Cell Sci. 124 (2011) 2511. https://doi.org/10.1242/jcs.095455.

[34] S. Tiwary, A. Nandwani, R. Khan, M. Datta, GRP75 mediates endoplasmic reticulum-mitochondria coupling during palmitate-induced pancreatic β-cell apoptosis, J. Biol. Chem. 297 (2021) 101368. https://doi.org/10.1016/j.jbc.2021.101368.

[35] E.A. Grzybowska, Calcium-binding proteins with disordered structure and their role in secretion, storage, and cellular signaling, Biomolecules. 8 (2018). https://doi.org/10.3390/biom8020042.

[36] A.C. Sotomayor-Pérez, D. Ladant, A. Chenal, Calcium-induced folding of intrinsically disordered Repeat-in-Toxin (RTX) motifs via changes of protein charges and oligomerization states, J. Biol. Chem. 286 (2011) 16997–17004. https://doi.org/10.1074/jbc.M110.210393.

[37] A. Chenal, J.C. Karst, A.C. Sotomayor Pérez, A.K. Wozniak, B. Baron, P. England, D. Ladant, Calcium-induced folding and stabilization of the intrinsically disordered RTX domain of the CyaA roxin, Biophys. J. 99 (2010) 3744–3753. https://doi.org/10.1016/j.bpj.2010.10.016.

[38] M. Sriram, J. Osipiuk, B.C. Freeman, R.I. Morimoto, A. Joachimiak, Human Hsp70 molecular chaperone binds two calcium ions within the ATPase domain, Structure. 5 (1997) 403–414. https://doi.org/10.1016/S0969-2126(97)00197-4.

[39] G. Szalai, G. Csordás, B.M. Hantash, A.P. Thomas, G. Hajnóczky, Calcium signal transmission between ryanodine receptors and mitochondria., J Biol Chem. 275 (2000) 15305-15313. https//doi.org/10.1074/jbc.275.20.15305.

[40] R. Rizzuto, D. De Stefani, A. Raffaello, C. Mammucari, Mitochondria as sensors and regulators of calcium signalling., Nat. Rev. Mol. Cell Biol. 13 (2012) 566–578. https://doi.org/10.1038/nrm3412.

Figure legends

Fig. 1 Effect of VES on mitochondrial Ca^{2+}

B16F1 cells were separately treated with 75 μM VES containing liposomes and 50 μM 2-APB for 6 h. Cells were pre-treated with 2-APB for 30 min prior to adding VES in the case of the VES+2-APB group. Mitochondria were detected with MitoTracker, and intracellular Ca^{2+} was detected with Fluo-4. (A) Structure of VE and VES. (B) Mitochondria (red) and Ca^{2+} (green) were observed after the noted treatments. Yellow fluorescence in the merged images represents mitochondrial Ca^{2+} levels; Scale bar = 20 μm. Magnified images of selected fields (white rectangles) are showing on the right (C) Relative yellow fluorescence intensity. Data are shown as mean ± SD (n = 3). ***, $P < 0.001$ (one-way ANOVA; Tukey's post hoc test).

Fig. 2 Rhodamine 2, AM assay for mitochondrial Ca^{2+}

B16F1 cells were separately treated with 75 μM VES containing liposomes and 50 μM 2-APB for 6 h. Cells were pre-treated with 2-APB for 30 min prior to adding VES in the case of the VES+2-APB group. (A) Mitochondria specific fluorescence (green) representing Ca^{2+} were observed after the noted treatments; Scale bar = 20 μm. (B) Relative green fluorescence intensity. Data are shown as mean ± SD (n = 3). *, $P < 0.05$ (one-way ANOVA; Tukey's post hoc test).

Fig. 3 Effect of VES on ER-mitochondria contact site formation

B16F1 cells were separately treated with 75 μM VES containing liposomes and 50 μM 2-APB for 6 h. Cells were pre-treated with 2-APB for 30 min prior to adding VES in the case of the VES+2-APB group. Mitochondria were detected with MitoTracker, and then cells were fixed and permeabilized prior to staining with an ER-specific fluorophore, Cytopainter. (A) Mitochondria (red) and ER (green) were observed after the noted treatments. Nuclei were counterstained with DAPI (blue). Yellow fluorescence in the merged images represents regions of ER-mitochondria contact; Scale bar = 20 μm. Magnified images of selected fields (white dotted rectangles) are showing on the right (B) Relative yellow fluorescence intensity. Data are shown as mean ± SD (n = 3). *, $P < 0.05$ (one-way ANOVA; Tukey's post hoc test).

Fig. 4 TEM analysis of VES induced MAM formation

TEM images of B16F1 cells treated with 75 μM VES for 6 h. (A) Magnified images of selected field (white dotted rectangles) are shown on the right. White arrow indicates ER; black arrow indicates mitochondria; Scale bar = 1 μm. (B) Box and whisker plot showing distance (μm) between ER and mitochondria (n=165 sites). ***, P<0.001 (unpaired Student's t-test).

Fig. 5 Effect of VES and 2-APB on GRP75 expression

B16F1 cells were treated with 75 μM VES-containing liposomes and 50 μM 2-APB. Cells were pre-treated for 30 min with 2-APB prior to the addition of VES in the case of the VES+2-APB group. (A) Total RNA was isolated after 6 h of treatment, and quantitative real time-PCR was performed (n = 3). Shown are levels of the mRNA encoding GRP75 normalized to the housekeeping gene *GAPDH*. (B) GRP75 protein in

cellular lysates was detected with western blotting, with β-actin serving as an internal control. (C) The intensities of protein bands shown in panel (B) were quantified with ImageJ. Data are shown as mean ± SD (n = 4). *, $P < 0.05$; **, $P < 0.01$, ***, $P < 0.001$ (one-way ANOVA; Tukey's post hoc test).

Fig. 6 Effect of VES on GRP75 localization

B16F1 cells were separately treated with 75 μM VES-containing liposomes and 2-APB for 3 h. Cells were fixed and permeabilized prior to immunostaining with an anti-GRP75 antibody and an Alexa Fluor 488-conjugated secondary antibody. The cells were counter-stained with the ER detection reagent Cytopainter. (A) GRP75 (green) and ER (red) were observed after the noted treatments. Magnified images of selected field (white dotted rectangles) showing the tubular network of the ER are shown on the right. Yellow fluorescence in the merged images represents colocalization of GRP75 and ER; Scale bar = 20 μm. (B) Quantification of the efficiency of colocalization of GRP75 and ER in the different treatment groups. Pearson's correlation coefficients were calculated using ImageJ software. Data are shown as mean ± SD (n = 3). ***, $P < 0.001$ (Kruskal-Wallis test; Dunn's post hoc test).

Fig. 7 Effect of VES on apoptosis induction

B16F1 cells were treated with 75 μM VES-containing liposomes and 50 μM 2-APB. Cells were pre-treated for 30 min with 2-APB prior to the addition of VES in the case of the VES+2-APB group. Nucleus were (A) White arrows indicate morphologically changed nucleus; Scale bar=20μm (B) Percentage of morphologically changed (apoptotic) nuclei; n=3; ***, P<0.001 (One way ANOVA; Tukey's post hoc test) (C) VES treated cells showed cell shrinkage, chromatin condensation (black arrow) of the

nucleus and cytoplasmic vacuoles (white arrow); magnified image of selected field (white dotted rectangles) is shown on the right; Scale bar = 20 μm.

Figure 1

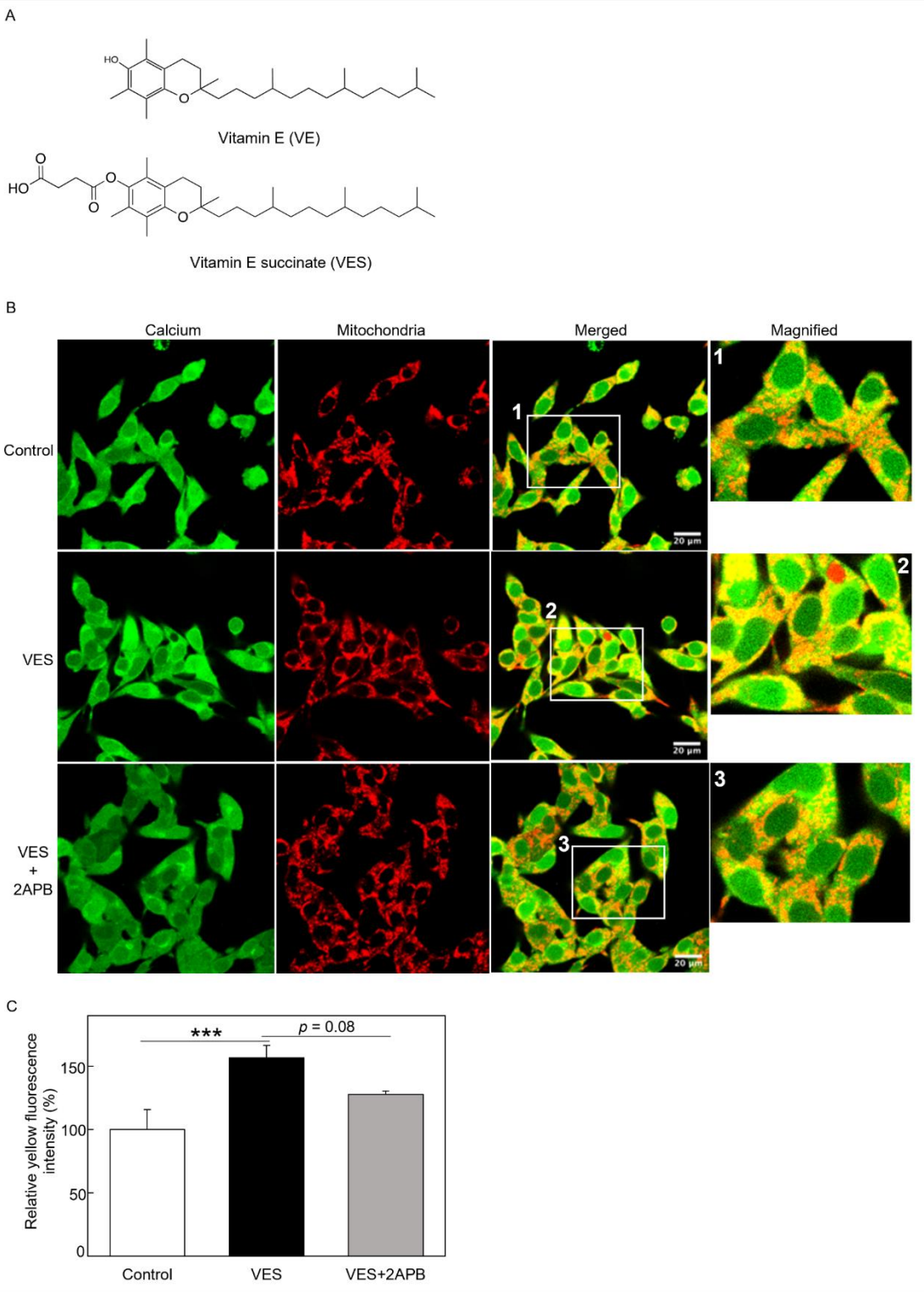
A
HO
O
Vitamin E (VE)
HO
O
O
O
O
Vitamin E succinate (VES)
B
Calcium
Mitochondria
Merged
Magnified
Control
VES
VES + 2APB
1
2
3
20 μm
C
Relative yellow fluorescence intensity (%)
***
p = 0.08
150
100
50
0
Control
VES
VES+2APB

Figure 2

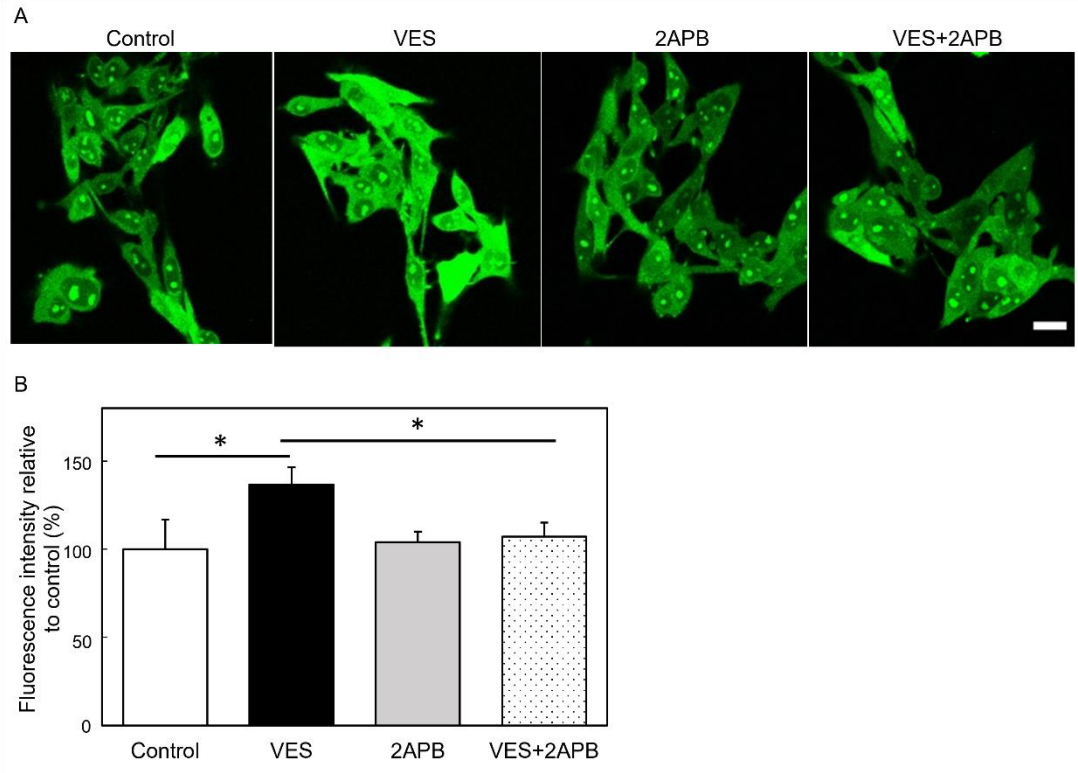
A
Control
VES
2APB
VES+2APB
B
Fluorescence intensity relative to control (%)
150
100
50
0
*
*
Control
VES
2APB
VES+2APB

Figure 3

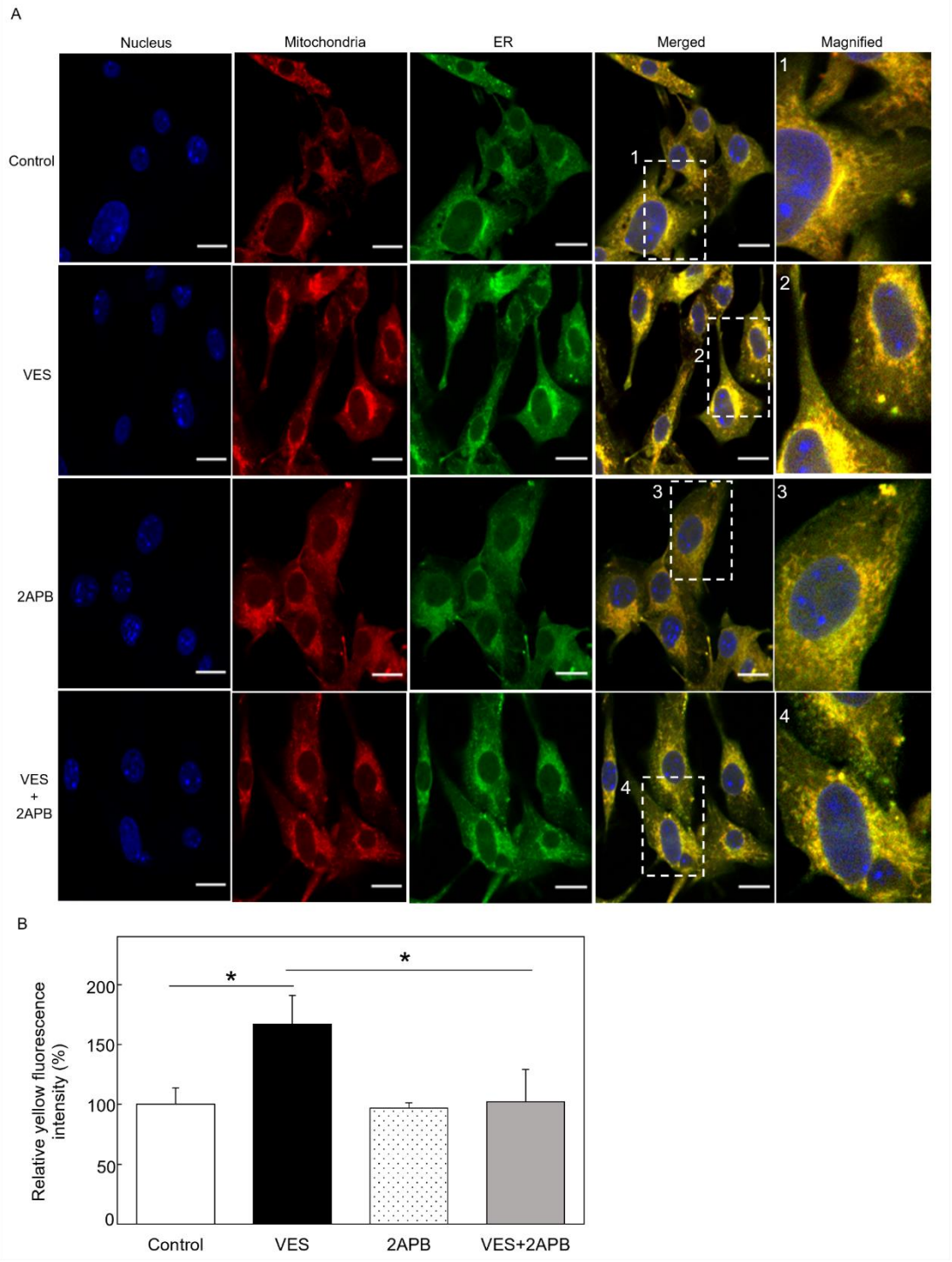
A
Nucleus
Mitochondria
ER
Merged
Magnified
Control
VES
2APB
VES + 2APB
1
2
3
4
B
Relative yellow fluorescence intensity (%)
200
150
100
50
0
*
*
Control
VES
2APB
VES+2APB

Figure 4

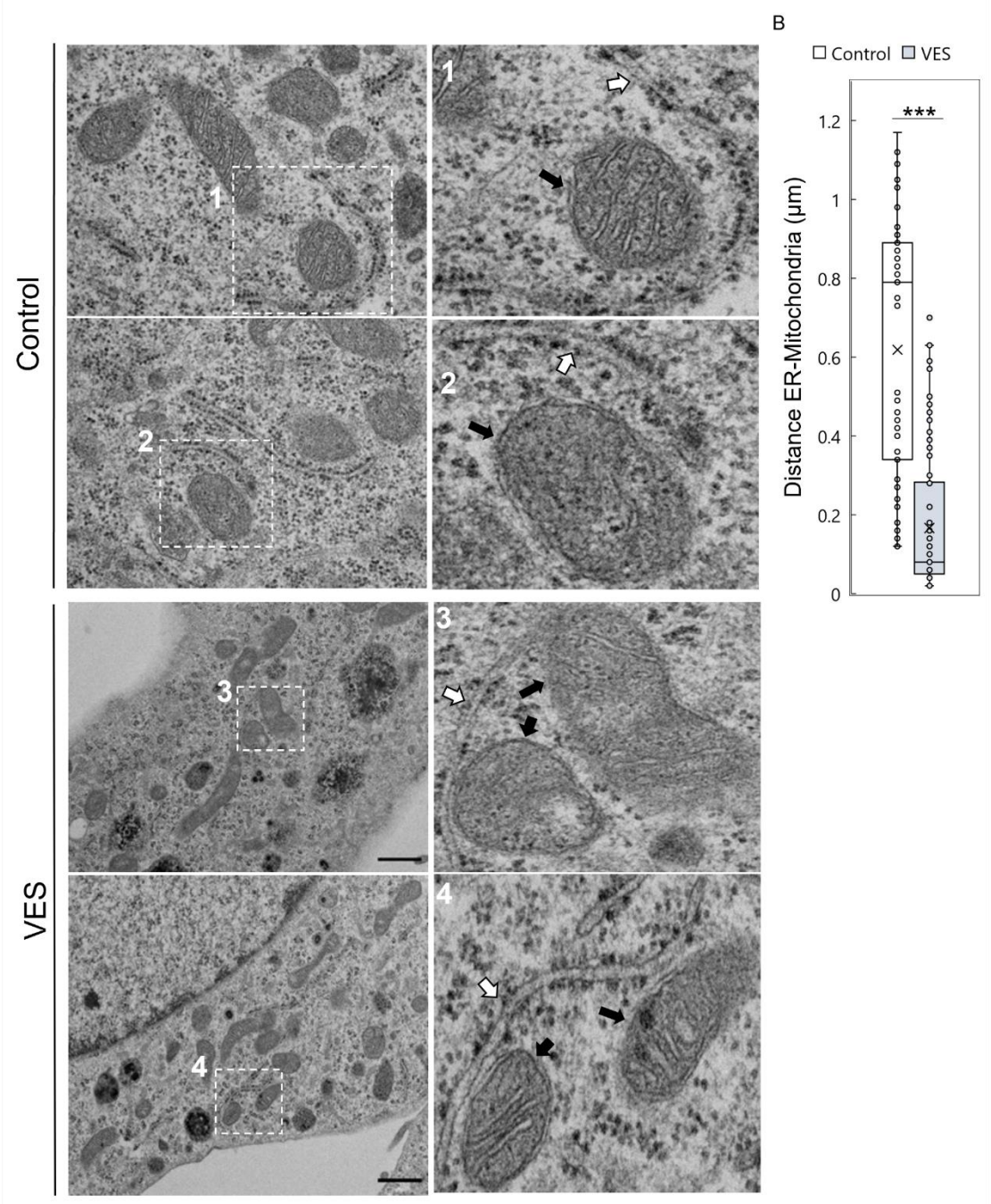
Control
VES
1
2
3
4
B
Control
VES
***
Distance ER-Mitochondria (µm)
0
0.2
0.4
0.6
0.8
1
1.2

Figure 5

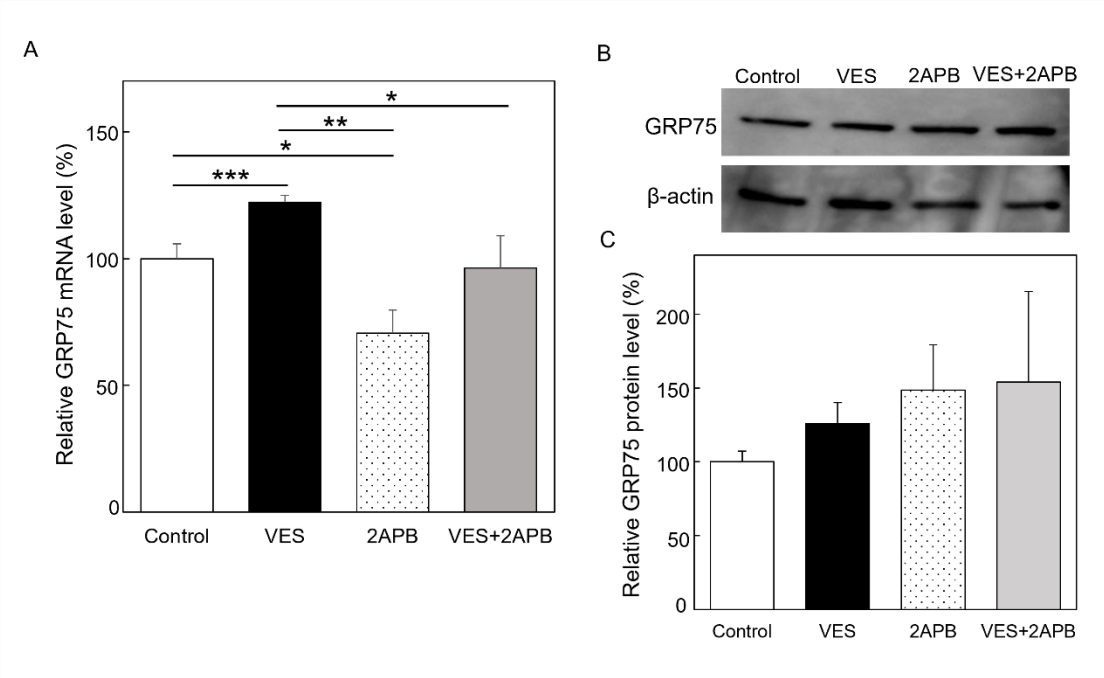
A
Relative GRP75 mRNA level (%)
150
100
50
0
***
*
**
*
Control
VES
2APB
VES+2APB
B
Control
VES
2APB
VES+2APB
GRP75
β-actin
C
Relative GRP75 protein level (%)
200
150
100
50
0
Control
VES
2APB
VES+2APB

Figure 6

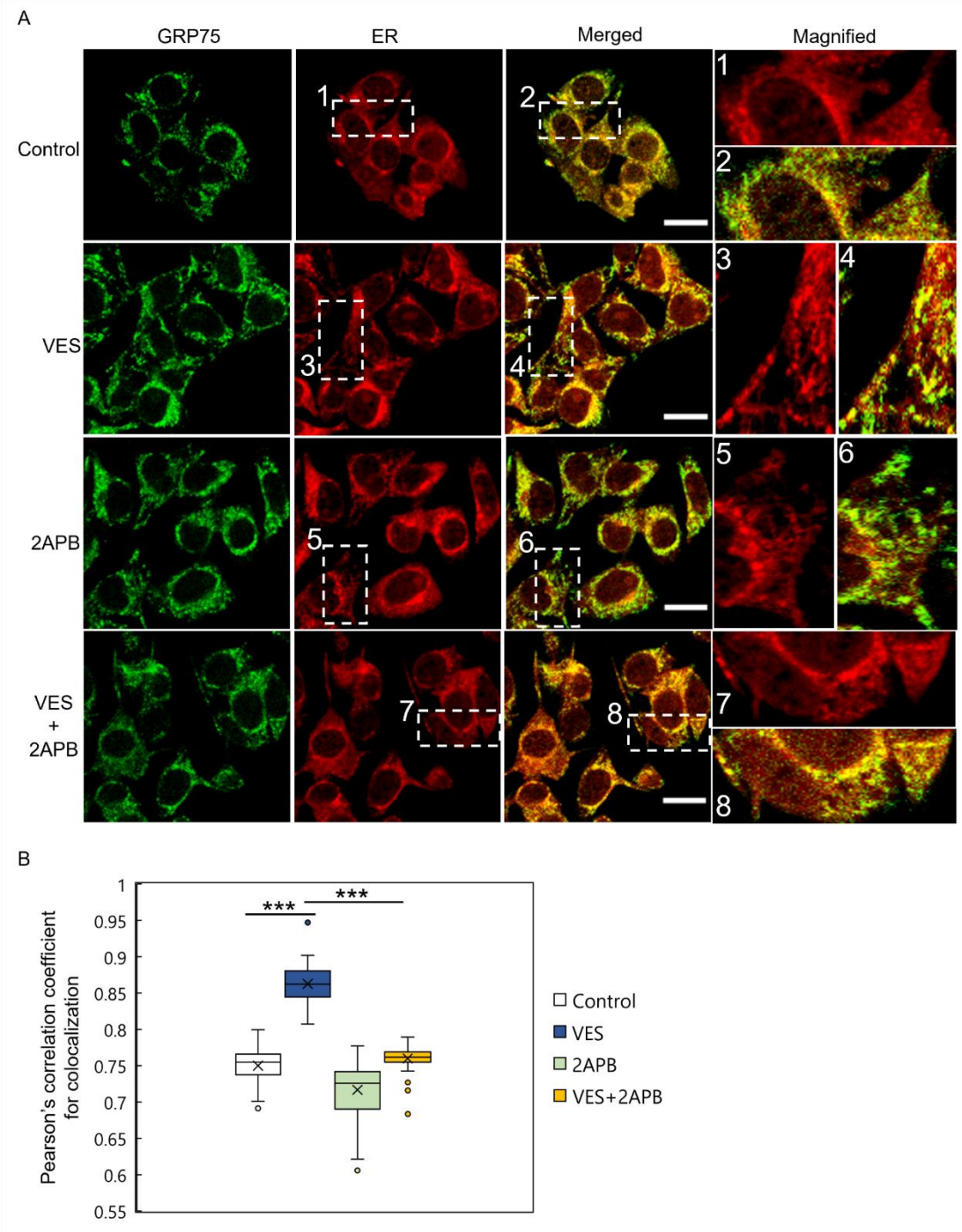
A
GRP75
ER
Merged
Magnified
Control
VES
2APB
VES + 2APB
1
2
3
4
5
6
7
8
B
Pearson's correlation coefficient for colocalization
1
0.95
0.9
0.85
0.8
0.75
0.7
0.65
0.6
0.55
***
***
Control
VES
2APB
VES+2APB

Figure 7

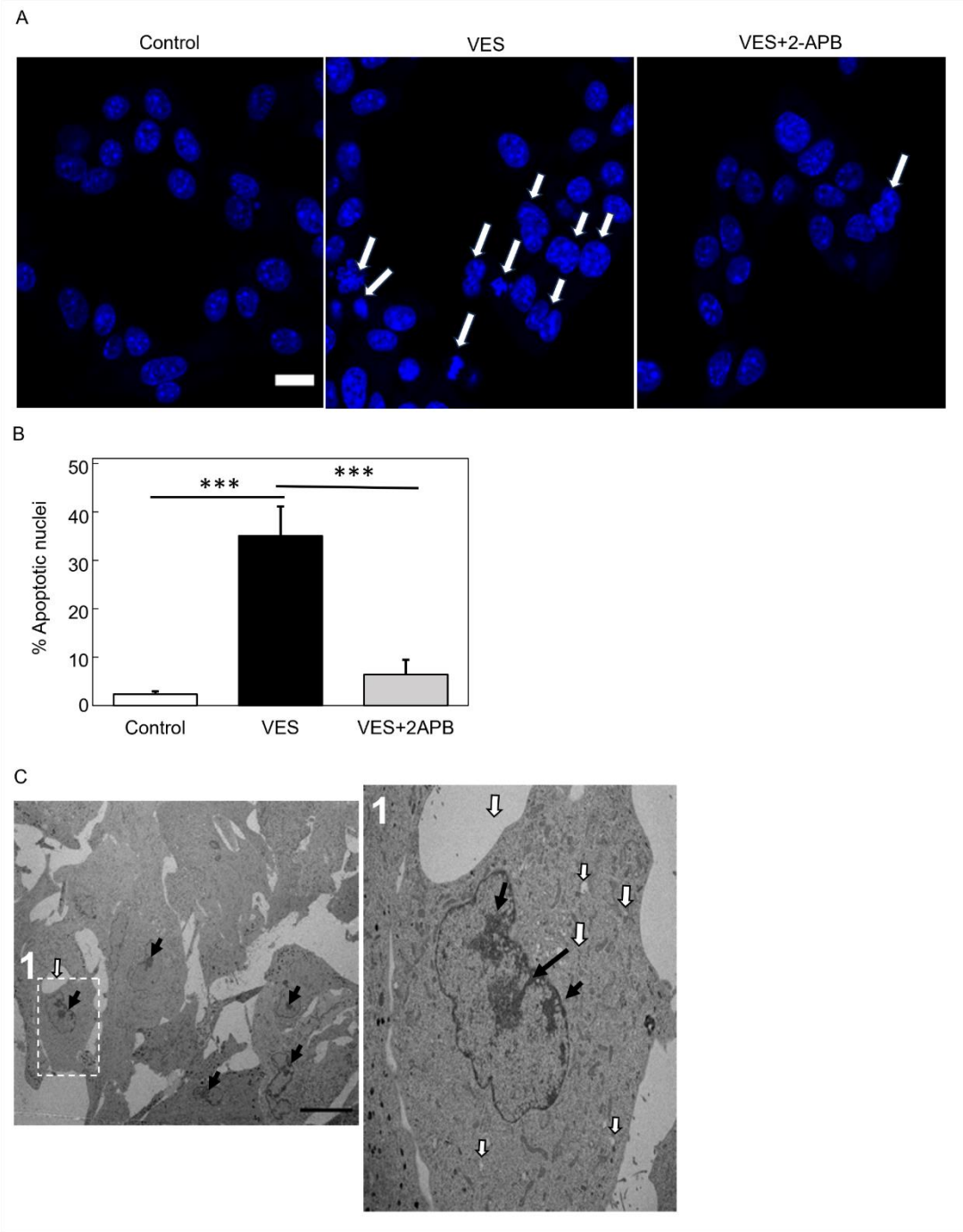
A
Control
VES
VES+2-APB
B
% Apoptotic nuclei
50
40
30
20
10
0
***
***
Control
VES
VES+2APB
C
1
1

Supplementary figure 1

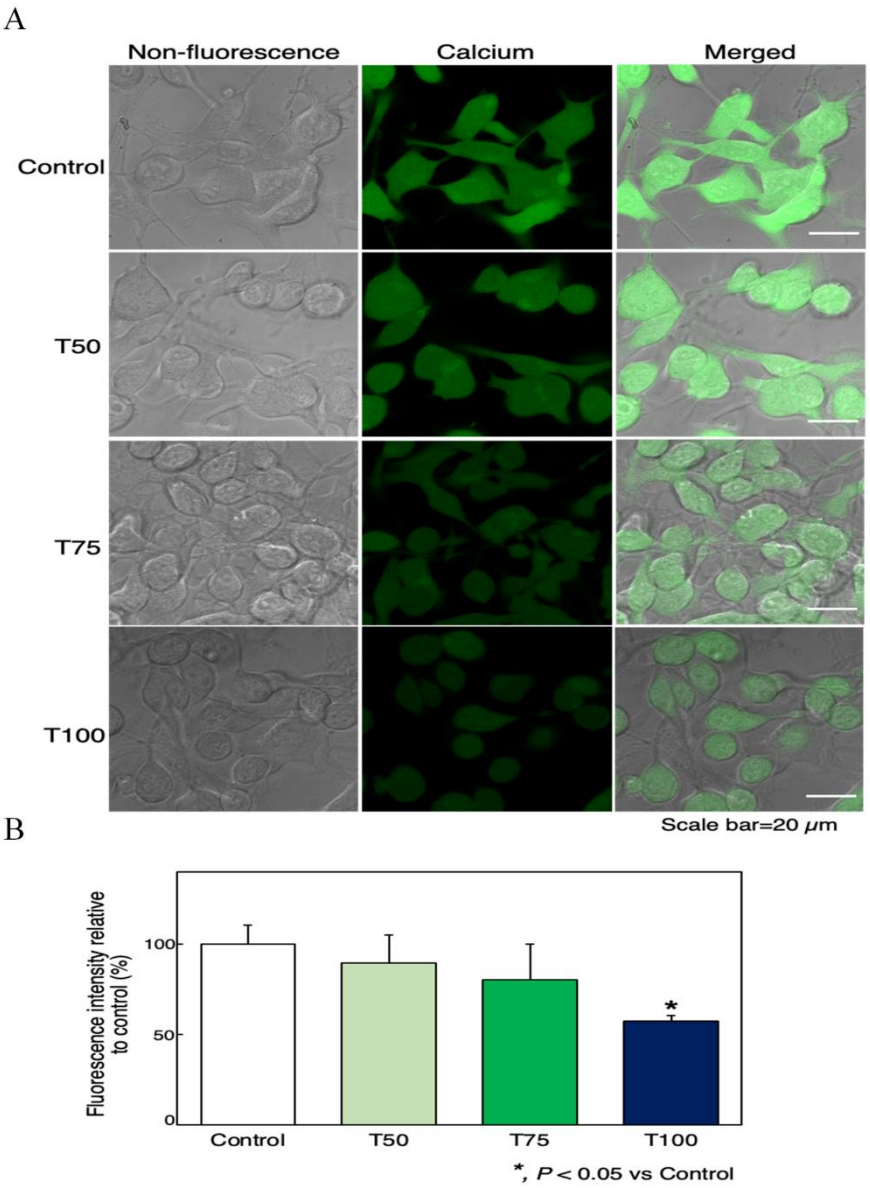

Supplementary Figure 1
Effect of VE on intracellular calcium level.
(A) A fluorescent indicator (Fluo4) was used to detect intracellular Ca^{2+} in B16F1 cells after treatments. (B) The fluorescence intensity was quantified by ImageJ. Data are shown as mean ± SD (n = 3). *p < 0.05, **p < 0.01 relative to control; #p < 0.05 (one way ANOVA; Tukey's Post hoc test). T50, T75 and T100 indicate 50 μM, 75 μM and 100 μM VE, respectively.

Supplementary figure 2

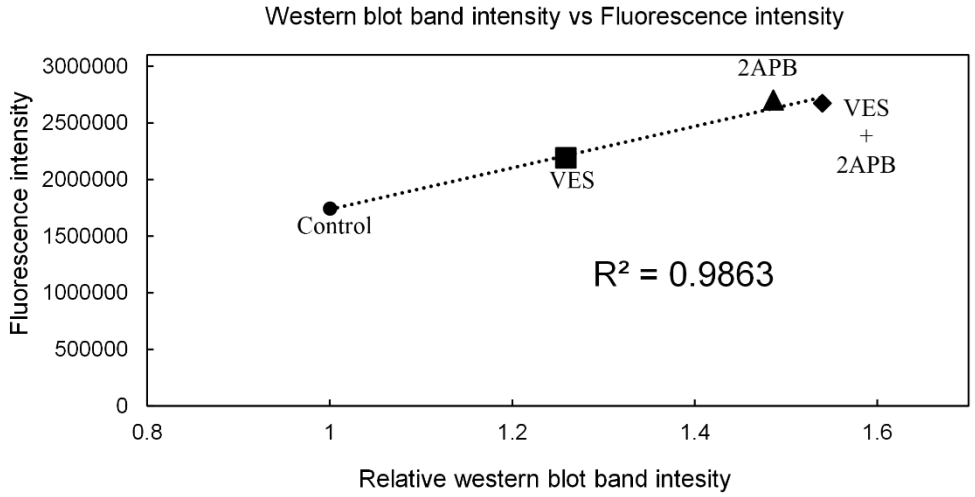

Supplementary Figure 2
Correlation between the fluorescence intensity of GRP75 and plotted against its western blot band intensity of the corresponding treatment groups.
Coefficient value of fluorescence intensity and relative western blot band intensity was R^2 = 0.9863.